Weather and Climate Extremes 3 (2014) 47–53

Contents lists available at ScienceDirect

Weather and Climate Extremes

journal homepage: www.elsevier.com/locate/wace

Predictability and prediction of decadal hydrologic cycles: A case study in Southern Africa

Vikram M. Mehta *, Hui Wang [1], Katherin Mendoza, Norman J. Rosenberg

Center for Research on the Changing Earth System, Catonsville, MD 21228, USA

ARTICLE INFO

Article history:
Received 18 September 2013
Received in revised form
3 April 2014
Accepted 4 April 2014
Available online 21 April 2014

Keywords:
Decadal climate variability
Decadal hydrologic cycle
Decadal droughts
Drought prediction
Earth System Models

ABSTRACT

Decision makers in drought-prone regions of the world and in international organizations responsible for drought relief require advance information, preferably on the decadal timescale, of future hydrometeorological conditions. Focusing on Southern Africa (SA), a region subject to droughts, we used indices of four decadal climate variability phenomena, statistically associated with Self-calibrating Palmer Drought Severity Index (SC-PDSI), hindcast/forecast by the MIROC5 Earth System Model from 1961 to 2019–2020, in a statistical prediction system (SPS) to assess SC-PDSI predictability. The SA-averaged correlation coefficient between hindcast and observations-based SC-PDSI increased from 0.2 in the 1980s to 0.33 in the 2001 to 2009–2010 period; grid point correlations within SA increased from 0.4 to over 0.7 during the last 30 years. The MIROC5 – SPS system forecasts that SA may experience a moderate drought from 2014 to 2016, followed by a wet period around 2019. These hydrologic event forecasts are predicated on the absence of major low-latitude volcanic eruptions during the prediction period.

1. Introduction

Multiyear to decadal hydrologic cycles (DHCs), with dry and wet parts, affect infrastructure, electricity generation, river navigation, recreation, urban water systems, crop production, pasture and range conditions, livestock production and health, ecological integrity, and regional and national economies (e.g., Mehta et al., 2013a). Recognition by decision-makers of the increasing societal consequences of DHCs has prompted legislation at the local, state and national levels encouraging water management and use efficiency. Floods cause loss of life and property in coastal regions and low-lying lands, and cause public health hazards that threaten the lives of survivors. However, the effects of multiyear to decadal droughts are particularly dramatic, resulting in billions of dollars in crop losses around the world annually. Droughts affect more people worldwide than any other natural hazard (Wilhite, 2000). Shortages of water for drinking and irrigation, consequent reductions in food production, and other stresses due to drought contribute to social and political strife, civil wars, and international conflicts (Gleick, 1993; Cooley et al., 2013). The negative consequences of long-duration droughts will intensify as growing numbers of humans and domesticated animals increase demands on available water supplies. The Final Declaration[2] of the recent United Nations sponsored High-level Meeting on National Drought Policy recognizes the need for and provision of drought information to affected countries and regions, and for help in the development of national drought policies. In addition to the need for information in times of immediate drought emergency, planning for water, food, energy, and urban infrastructure development would benefit greatly from reliable information on prospects for wet and dry periods extending two or more decades into the future. If skillful forecasts of this kind are to be possible, the causes of DHCs must be better understood.

A substantial body of research has emerged in the last two decades, focused on understanding causes and mechanisms of decadal climate variability (DCV) (Meehl et al., 2009; Murphy et al., 2009) and its influences on terrestrial hydrology. Several DCV phenomena – the Pacific Decadal Oscillation (PDO) (Mantua et al., 1997; Minobe, 1997), tropical Atlantic Sea-surface Temperature

* Correspondence to: Center for Research on the Changing Earth System, 5523 Research Park Drive, Suite 315, Catonsville, MD 21228, USA. Tel.: +1 443 543 5493.
E-mail addresses: vikram@crces.org, mehtavm@yahoo.com (V.M. Mehta), huiwang@crces.org (H. Wang), mendoza@crces.org (K. Mendoza), normjrosenb@crces.org (N.J. Rosenberg).
[1] Also at Wyle ST&E Group and NOAA/Climate Prediction Center, Camp Springs, MD, USA.

[2] www.hmndp.org.

http://dx.doi.org/10.1016/j.wace.2014.04.002

(SST) gradient variability (TAG) (Houghton and Tourre, 1992; Mehta and Delworth, 1995; Chang et al., 1997; Mehta, 1998), West Pacific Warm Pool Variability (WPWP) (Wang and Mehta, 2008), and decadal variability of El Niño-La Niña cycles (Balmaseda et al., 1995; Power et al., 1999; An and Wang, 2000; Kestin et al., 1998) – have been identified in observational records and associated with the occurrence of DHCs on land (Mehta, 1998; Nigam et al., 1999; Hidalgo, 2004; McCabe et al., 2004; Meehl and Hu, 2006; Schubert et al., 2009; Mehta et al., 2011). While simulation experiments with global Earth System Models (ESMs) have substantially clarified and reproduced the hypothesized role of DCV phenomena in DHCs in some regions of the world (Schubert et al., 2009), skillful predictions of DCV influences on DHCs remain elusive.

Despite problems in understanding and prediction of DCV, but encouraged by initial decadal climate predictability studies with ESMs (Latif et al., 2006; Smith et al., 2007; Keenlyside et al., 2008; Pohlmann et al., 2009), the World Climate Research Program organized the Coupled Model Intercomparison Project 5 (CMIP5) to assess the ability of the current generation of ESMs used in climate and impacts assessments by the Inter-Governmental Panel on Climate Change to simulate and hindcast (retrospectively forecast) decadal climate. Significant and substantial hindcast skill has been found in SSTs averaged in ocean basins (Mehta et al., 2013b), as well as in SST indices associated with DCV phenomena with multiyear to decadal lead times in decadal hindcast runs of several ESMs made under CMIP5 (Mehta et al., 2014). One consideration, however, is that, in CMIP5 experiments, major low-latitude volcanic eruptions have been found to influence SSTs; actually, the eruptions are one of the sources of decadal SST hindcast skill due to the radiative influence of ejected materials on low-latitude, upper-ocean heat budget and SSTs, and the subsequent slow recovery of the SSTs towards their pre-eruption state (Mehta et al., 2013b, 2014). In the real world, however, volcanic eruptions are not yet predictable. Therefore, their effects on the climate system can only be predicted *ex post facto*. Nevertheless, to exploit the degree of prediction skill demonstrated, we have developed a statistical prediction system (SPS) for rainfall, temperature, drought index, and other features of DHCs on land. An application of the SPS for DHC prediction and assessing its accuracy in hindcasting DHCs in Southern Africa, a major drought-prone region of the world, is described in this paper as a case study. As described later, DHCs in Southern Africa show moderate to high correlations with some of the DCV indices, and atmospheric conditions associated with positive and negative phases of DCV indices are physically consistent with DHC variability.

2. Material and methods

Two sets of core decadal prediction experiments are conducted under CMIP5 (Meehl et al., 2009). The first set is a series of 10-year hindcasts starting approximately in 1960, 1970, 1980, 1990, and 2000. The second is a series of 30-year hindcasts starting in 1960, 1980, and 2005, the last a combined hindcast–forecast. In both sets, aerosol optical depths (AODs, including those due to volcanic eruptions) and solar radiation are prescribed from past observations. Each experiment has a minimum ensemble size of three members. These experiments are somewhat idealistic and exploratory, especially in view of the well-known difficulty of predicting volcanic eruptions well in advance.

In this case study, the dynamical component of our hybrid prediction system is the Model for Interdisciplinary Research On Climate 5 (MIROC5) from Japan. MIROC5 was selected for this case study because our previous comparisons of decadal hindcast skills of four CMIP5 ESMs showed that MIROC5 has the best overall skill (Mehta et al., 2013b, 2014). The MIROC5 ESM is from Atmosphere and Ocean Research Institute (University of Tokyo), National Institute for Environmental Studies, and Japan Agency for Marine-Earth Science and Technology, Japan. It is a global model with an equivalent resolution of approximately 1.41° longitude–0.79° latitude. There are decadal hindcasts starting in 1961, 1971, 1981, 1991, and 2001, each running for 10 years after initialization. Generally, ESMs are chaotic dynamical systems, making hindcasts/forecasts made with them sensitive to initial conditions. Such sensitivity can induce hindcast/forecast runs to diverge significantly even if their initial conditions are infinitesimally close. This sensitivity to initial conditions necessitates conducting parallel hindcast/forecast runs of the same ESM initialized with slightly different values of oceanic and/or atmospheric variables in the ESM. Such a collection of runs is known as an ensemble and the average of the ensemble is considered a more accurate hindcast/forecast than any individual member of the ensemble. The spread of member hindcasts/forecasts is a measure of the overall hindcast/forecast skill. There are six members in each MIROC5 decadal hindcast ensemble. In the CMIP5 hindcast experiments, the MIROC5 used an ocean-only initialization scheme (Tatebe et al., 2012). In all CMIP5 experiments, Northern Hemisphere and Southern Hemisphere time series of aerosol optical depth (AOD), based on observations (Sato et al. (1993) and Hansen et al. (2002) in the MIROC5 ESM), were specified. These data sets provide zonal-average, vertically-resolved AOD for visible wavelengths and column-average effective radii of aerosols (Stenchikov et al., 2006). The CMIP5 decadal hindcasts made with the MIROC5 ESM form the dynamical component of the hybrid dynamical–statistical prediction system described here.

In the statistical component of the hybrid prediction system, we use four SST indices derived from MIROC5 decadal hindcasts – Niño 3.4, PDO, TAG, and WPWP SST indices – as the predictors. Precipitation, temperature, drought indices, and other weather/climate variables are the predictands. We begin by estimating correlation coefficients between monthly-, seasonal-, or annual-average of an observed predictand (say, precipitation) and each observed SST index, and between an observed predictand and each SST index from MIROC5 ensemble-average hindcasts. If an ESM is able to simulate the predictand reasonably well and hindcast the predictor with significant skill, we expect that the two correlation coefficient patterns may be similar to some extent. If the two patterns are very different, the SPS would not be able to hindcast the predictand with any skill. The SPS consists of the following four steps.

Step 1: Multiple, linear regression of the observed predictand (for example, a drought index) vs. the four SST indices from the ESM based on the data from 1961 to 2010, but taking out the 1981 to 1990 data.
Step 2: Prediction of the drought index for the 1980s, using the multiple, linear regression model constructed in Step 1 and SST index hindcasts for the 1980s.
Step 3: Repeat Steps 1 and 2 for predicting drought index for each decade.
Step 4: Cross-validation – estimate correlation coefficient between observed and predicted drought index from 1961 to 2010.

We selected the Self-calibrating Palmer Drought Severity Index (SC-PDSI; Wells et al., 2004) as an indicator of DHC. The original PDSI is based upon a primitive water balance model (Palmer, 1965). The basis of the PDSI is the difference between the amount of precipitation required to retain a normal water-balance level and the amount of actual precipitation. The other parts of the PDSI calculation account for climatic differences between locations and seasons of the year. These computations attempt to scale the index

values so that they fit 11 dryness/wetness categories (Palmer, 1965) and allow for comparisons across time and space. Empirical constants for climatic characteristic and duration factors used in the computation of the PDSI, which directly affect the spatial comparability of the index, are based on averaging the values from only a few locations in western Kansas and central Iowa representing a small number of climates. The SC-PDSI replaces the empirically derived climatic characteristic and duration factors with values based on the historical climatic data of each location, thereby making the SC-PDSI more representative of the location and its climate (Wells et al., 2004). We obtained monthly 2.5° longitude–2.5° latitude gridded SC-PDSI dataset from 1960 to 2010 from http://www.cgd.ucar.edu/cas/catalog/climind/pdsi.html. The SC-PDSIs in many locations show drying or moistening trends from 1960 to 2009–2010. Our hybrid system is used to predict SC-PDSI before and after detrending in order to assess hindcast skill due to multidecadal trends and DCV phenomena.

The "goodness of fit" (GoF) of the regression model to observed data was estimated with the *R*-squared test (Press et al., 1992) and the statistical significance of regression coefficients was tested with the *T*-test (Press et al., 1992). In order to assess GoF, an *R*-squared test was performed on each of the regressed combinations of SC-PDSI and the four DCV indices. When the data of interest are regressed linearly, the *R*-square test is simply the square of the sample correlation coefficient between the outcome (SC-PDSI) and the values being used to predict the outcome (DCV index). The *R*-squared values can vary from 0 to 1, indicating how well the regression line approximates the SC-PDSI data points – that is the GoF. The *R*-squared value represents the percent of variance in the values of SC-PDSI that can be explained by knowing the value of a DCV index, with a value of 0 indicating no variance explained and a value of 1 indicating all variance explained. Therefore, the greater the R^2 value, the more the explained variance. In the present analysis, *R*-squared values ranged from 0.5 to 0.7 over much of SA, indicating a satisfactory model fit. In addition to the GoF test, a *T*-test was also performed to determine statistical significance of the estimated regression coefficients. The *T*-statistic is obtained by dividing the slope of the regression line by the standard error. Values above or below 2.011 indicate a relationship significant at the 95% confidence level between the independent variable (a DCV index) and the dependent variable (SC-PDSI). The same area-averaging as the *R*-square test for representing SA was applied to *T*-test values. It was found that patterns of 95% significance were similar to those of the R^2 values. At specific locations, this was also evident with all significant *T*-test areas coinciding with *R*-square areas with the latter values approximately greater than or equal to 0.5. This coincidence showed that where the regression models had an acceptable GoF, they also had statistically significant regression coefficients encompassing SA. We interpreted these GoF and *T*-test indicators as sufficiently indicative for this exploratory study.

The Monte Carlo technique (e.g., Wilks, 1995) was used to estimate statistical significance of correlation coefficients. Hindcast skills as indicated by correlation coefficient and root-mean-square error are described in this paper. Correlation coefficients equal to or greater than 95% confidence limit are referred to as statistically significant in this paper. Also, negative correlation coefficients are referred to as negative skill.

We used the Extended Reconstructed SSTs (ERSST; Reynolds et al., 2002) from 1961 to 2010 for comparison with hindcast SSTs.

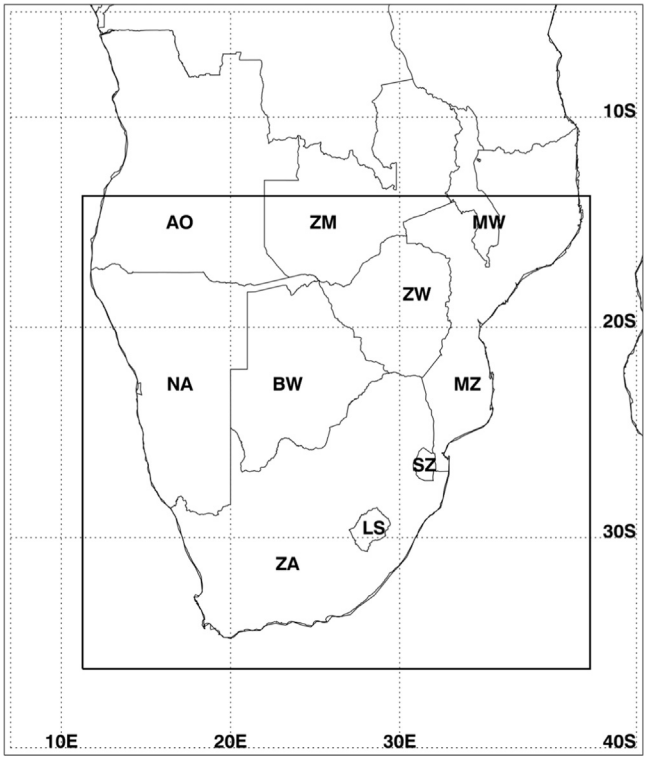

Fig. 1. The Southern Africa region of this study with two-letter country identifiers: AO – Angola, ZM – Zambia, MW – Malawi, ZW – Zimbabwe, NA – Namibia, BW – Botswana, MZ – Mozambique, SZ – Swaziland, LS – Lesotho, and ZA – South Africa.

3. Results

An application of the hybrid system to predict DHCs in SA is described here; all or parts of 10 countries between approximately 14°S and 35°S latitudes are included as shown in Fig. 1. SA is mostly semi-arid, with pronounced decadal variability in rainfall (Tyson, 1986). SA is also projected to experience increased variability in rainfall and, possibly, reduced precipitation and increased evaporation as a result of anthropogenic climatic change. With a growing population[3,4] and increasing demand for water from numerous sectors, freshwater availability is a high-priority concern for SA. In addition to decadal variability and a potential long-term decrease in precipitation, water security in SA is further complicated by high population densities in arid areas.[5]

Correlation coeffcients between observations-based SC-PDSI and PDO, TAG, WPWP, and Niño 3.4 indices during the October to March rainy season in SA in the 1961–1962 to 2009–2010 period are shown in Fig. 2. The PDO (Fig. 2a) has significant correlations at 95% (−0.4 and lower) with the SC-PDSI in Southern Angola, Southern Zambia, Namibia, Botswana, and South Africa, such that dry (wet) periods are associated with a positive (negative) PDO index. The TAG (Fig. 2b) is negatively correlated with SC-PDSI in Angola, Zambia, and Malawi at 90% significance, implying that dry (wet) periods are associated with a positive (negative) TAG index. The WPWP variability (Fig. 2c) has correlations with SA SC-PDSI at 90% or lower significance. The Niño 3.4 index (Fig. 2d) has −0.4 and lower correlation coefficient in South Africa, Mozambique, and Zimbabwe at 95% level and lower correlations elsewhere in SA, implying that dry (wet) periods in these three countries are associated with El Niño (La Niña) events. Thus, Fig. 2 shows that SST indices of the four DCV phenomena are associated with droughts and pluvials in large parts of SA with substantial statistical significance. Correlations between hindcast DCV indices and observations-based SC-PDSI show a reasonable similarity with

[3] http://www.aaas.org/international/ehn/waterpop/southaf.htm.
[4] http://www.worldpopulationstatistics.com/africa-population-2013/.
[5] www.unep.org/dewa/africa/publications/aeo-1/161.htm.

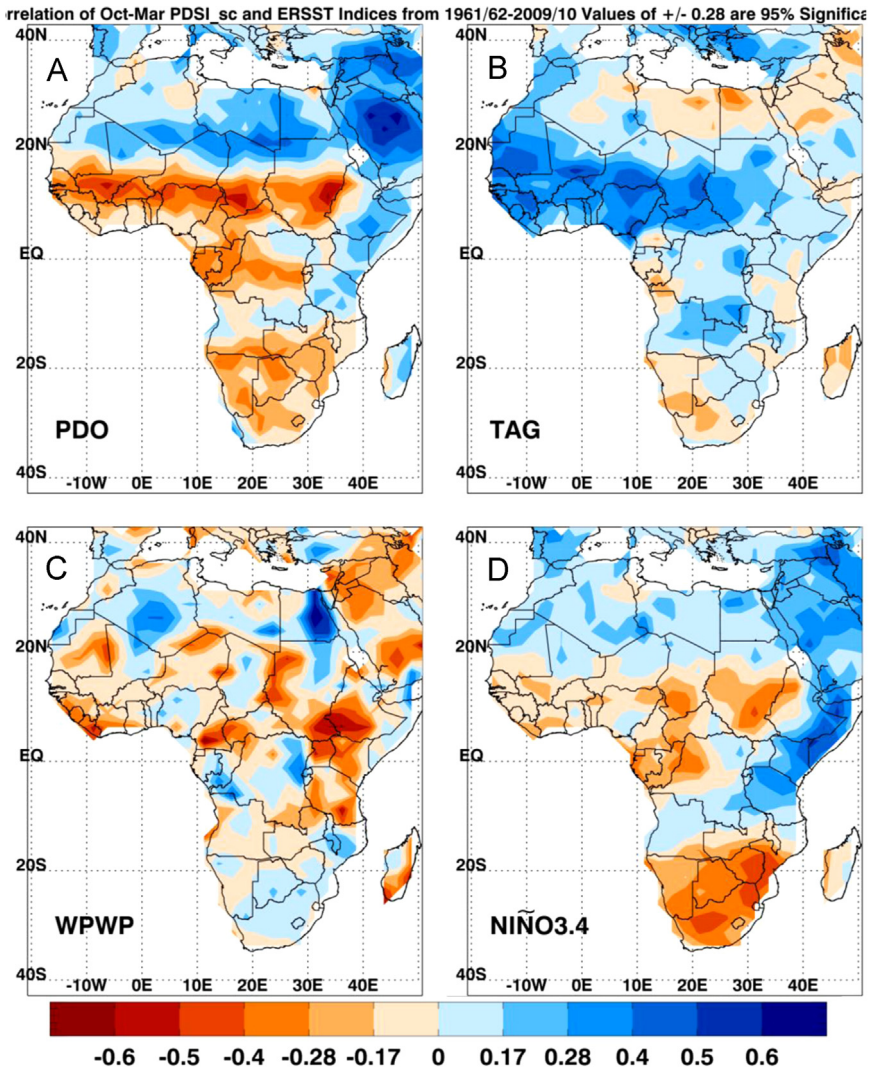

Fig. 2. Correlation coefficients between SC-PDSI and sea-surface temperature (SST) indices of (A) PDO, (B) TAG, (C) WPWP, and (D) Niño 3.4 averaged in the October–March rainy season in Southern Africa at 2.5° longitude–2.5° latitude grid spacing from 1961–1962 to 2009–2010. The threshold for 95% significance is ± 0.28. The observed SST indices were calculated with the extended reconstructed SST (ERSST; Reynolds et al., 2002) data.

those in Fig. 2. Therefore, hindcast DCV indices can be used in the SPS to hindcast SC-PDSI.

Correlation coefficients between each of the four DCV indices, and 500-hPa geopotential heights and 850 hPa winds from the NCEP-NCAR reanalysis, averaged over the October–March period, during 1961–2010 suggest (not shown) consistency of these important atmospheric variables with the SC-PDSI correlation coefficients shown in Fig. 2. For example, when the PDO index is positive, there is an atmospheric wave train emanating from the tropical Pacific Ocean region and there are 850 hPa wind anomalies from interior land regions over SA, implying less atmospheric water flux coming to SA and possibly resulting in a dry period as implied by the negative SC-PDSI correlation in Fig. 2A. Generally similar atmospheric and SC-PDSI anomalies are found during the positive or El Niño phase of the Niño 3.4 index. During a positive phase of the TAG index (tropical North Atlantic SST anomalies warmer than tropical South Atlantic SST anomalies), the TAG SST pattern is associated with geopotential height and 850 hPa wind anomalies in the North and South Atlantic regions. Our results show that when the TAG index is positive, there are strong 850 hPa wind anomalies from the South Atlantic Ocean towards interior SA, especially Angola, Zambia, and parts of Malawi, implying more rain as indicated by the negative SC-PDSI correlation in these regions in Fig. 2B. In the positive phase of the WPWP SST variability, there are anomalous northwesterly 850 hPa wind anomalies from the South Atlantic to SA, suggesting more atmospheric water resulting in wetter SA, especially Botswana and parts of South Africa, as indicated by the SC-PDSI correlations in Fig. 2C.

The predicted and observations-based SC-PDSI anomalies, averaged in SA over the October–March rainy season, from 1961 to 2009–2010 are shown in Fig. 3. Both sets of anomalies are plotted as continuous time series. Since, in general, the SC-PDSI anomaly at the end of one decadal hindcast may not be close to the SC-PDSI anomaly at the beginning of the next decadal hindcast, there are visible discontinuities at the decadal hindcast boundaries. Fig. 3 shows that decadal variations in both after late 1970s–early 1980s are similar, especially the broad outlines of dry and wet periods in smoothed versions of the time series before or after detrending. Also, for almost the entire 50-year period, the observations-based SC-PDSI anomalies are within the ± 1 standard deviation band estimated from hindcasts with 6 individual members of the MIROC5 ensemble; and correlation coefficients between observations-based and hindcast SC-PDSI over the 50-year period are 0.39, 0.43, 0.46, and 0.53 (Fig. 3A-D, respectively). Amplitudes of the observations-based and hindcast SC-PDSI are

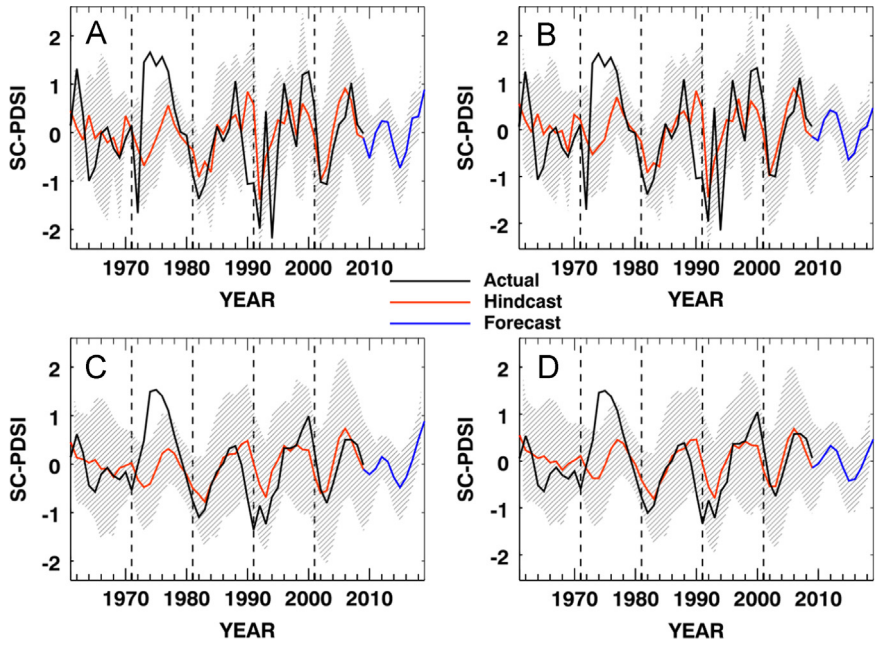

Fig. 3. Actual (black line) and ensemble-average hindcast (red line) from 1961 to 2009–2010 and forecast (blue line) SC-PDSI from 2010–2011 to 2019–2020, averaged over the October–March rainy season in Southern Africa. Cross-hatched area shows ± 1 standard deviation of hindcast/forecast SC-PDSI. Decadal hindcasts/forecasts of four sea-surface temperature (SST) indices of decadal climate variability – PDO, TAG, WPWP, and Niño 3.4, made with a six-member ensemble of the MIROC5 Earth System Model, were used in a cross-validated statistical prediction system to hindcast/forecast SC-PDSI. Start years of decadal hindcasts are shown with vertical dashed lines; the 2010–2011 to 2019–2020 forecasts were initiated in 2001. Results: (A) without detrending or smoothing, (B) after removing a linear trend spanning 1961–2010, (C) without detrending, but after smoothing by a three-year moving-window filter and (D) after removing a linear trend spanning 1961 to 2009–2010 and smoothing by a three-year moving-window filter. 1961 refers to the October 1961–March 1962 averaging time.

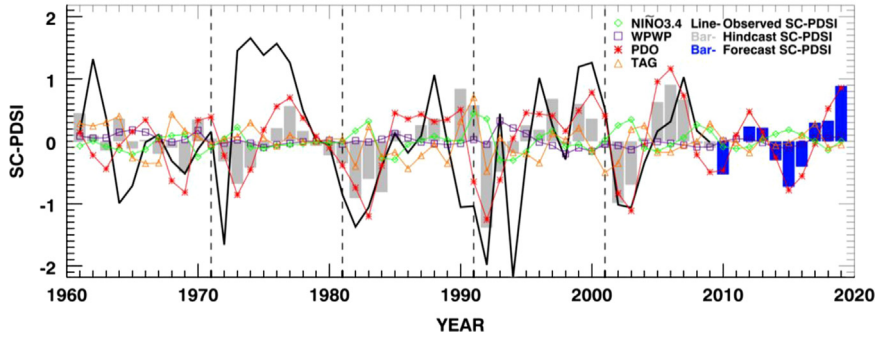

Fig. 4. Actual (heavy black line) and ensemble-average hindcast (gray bars) self-calibrating Palmer drought severity index (SC-PDSI) from 1961 to 2009–2010, and SC-PDSI forecast (blue bars) from 2010–2011 to 2019–2020, averaged over the October–March rainy season in Southern Africa. Contributions to hindcasts/forecasts of SC-PDSI anomalies by PDO, TAG, WPWP, and Niño 3.4 are also shown as per the legend in the box. Start years of decadal hindcasts are shown with vertical dashed lines; the 2010–2011 to 2019–2020 forecasts were initialized in 2006.

generally similar after the late 1970s, although, as expected, filtering and detrending (Fig. 3B–D) generally reduce their amplitudes. Another interesting result is that decadal hindcasts initiated at the beginning of each decade capture a dry period at the start, followed by a wet period near the end, followed by yet another dry period. Thus, the hindcasts after the late 1970s reproduce entire DHCs reasonably well. Year-to-year variability, however, is reproduced less well in the hindcasts than is decadal variability due, possibly, to the decadal character of PDO, TAG, and WPWP manifestations. As Fig. 4 shows, the PDO predictability contributes the most to predictability of the SC-PDSI, especially the phase. Niño 3.4 is next in predictive power, with minor contributions made by TAG and WPWP. This is also confirmed by predictions made by simple linear regression models based on only a single DCV predictor.

The apparent improvement in hindcasts over the 50 year period is also reflected in grid point correlation coefficients and root-mean-square (RMS) differences between observations-based and hindcast SC-PDSI anomalies shown in Fig. 5. An increase in correlation coefficients and their statistical significance, and decrease in RMS differences are also noted, especially after the 1980s, with the 1991–2000 (Fig. 5G and H) and 2001 to 2009–2010 (Fig. 5I and J) results showing significant and substantial correlations, and generally low RMS differences over almost the entire SA region. With a record of improving hindcast skill for the period following the 1980s, we used the MIROC5 hindcast–forecast for the 2006–2036 period to predict the evolution of SC-PDSI from 2011 to 2020 (Fig. 3). The hybrid system predicted a slightly wet period in 2011–2012, followed by a dry period in 2014–2016 and a wet period at the end of the decade. This forecast, of course,

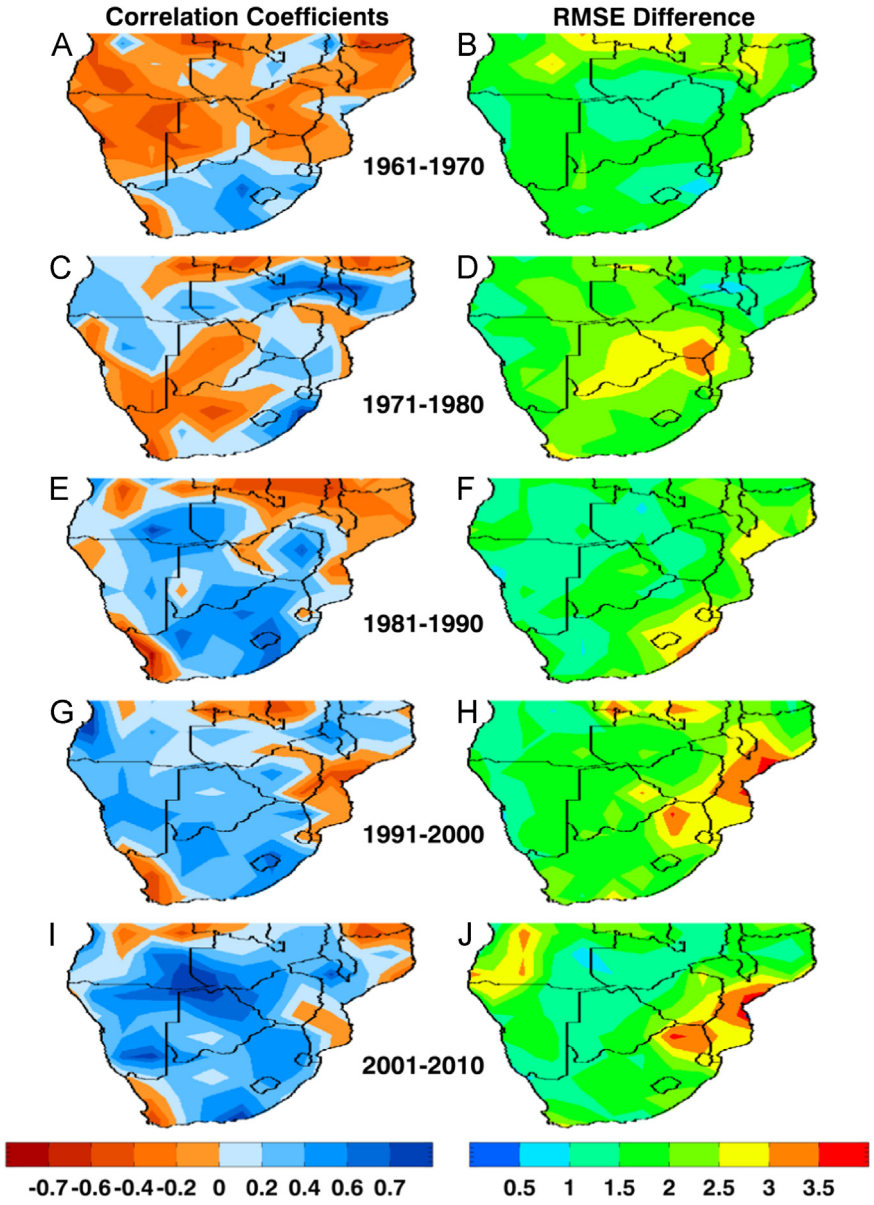

Fig. 5. Correlation coefficients and root-mean-square differences between actual and hindcast SC-PDSI from 1961 to 2009–2010, averaged over the October–March rainy season at 2.5° longitude–2.5° latitude grid spacing in Southern Africa. Color scales are shown below the figures. The thresholds for significance of correlation coefficients are ±0.63 for 95%, ±0.55 for 90%, ±0.49 for 85%, ±0.44 for 80%, and ±0.40 for 75%.

is subject to the caveat that any major low-latitude volcanic eruption during this period might influence DHC in SA.

4. Discussion and conclusions

The moderate success of the hybrid system in hindcasting DHCs in SA, as evidenced in the SC-PDSI, suggests that such cycles in this region are indeed forced largely by DCV phenomena. The moderate skill of the MIROC5 ESM in hindcasting the occurrence of the four DCV phenomena, especially PDO, explains the success in hindcasting DHCs during the past 3–4 decades. We speculate that improved observations to initialize ESMs, especially ocean observations, may be responsible for progressively improving hindcast skill in the 1960–2010 period in the CMIP5 ESMs as well as improvements in the ESMs themselves. It is remarkable that hindcast skill is not limited to the time immediately following MIROC5 initialization, but in some of the decades extends to the end of the 10-year hindcasting period, providing substantial skill over entire DHCs. While cognizant of the role of volcanic eruptions in determining decadal hindcast skill, the reasonably successful multidecadal record of decadal SC-PDSI hindcasting presented here encourages us to expect that the forecast from 2013 to 2020 will also be skillful.

Although preliminary results of this study are very encouraging, they must be viewed with caution because the CMIP5 decadal hindcast experiments use estimates of ejected volcanic materials and solar variability during hindcast periods that would not be available in making actual forecasts. An encouraging beginning, however, has been made on the long sought-after goal of decadal drought forecasts. While the climate modeling and prediction community further develop the ESMs and techniques for decadal drought prediction, it is vitally important that the climate services community develops models and techniques for prediction of societal impacts of multiyear to decadal droughts, and mechanisms and organizations for continuous interactions with stakeholders who would be the ultimate beneficiaries of decadal drought and impacts prediction.

Acknowledgments

This research is supported by the US Department of Agriculture-National Institute of Food and Agriculture under Grant 2011-67003-30213 in the NSF – USDA – DOE Earth System Modelling Program. The authors are grateful to Toru Nozawa (National Institue for Environmental Studies, Japan) for discussions about the CMIP5 experiments conducted with the MIROC5 model and about the aerosol data used in the CMIP5 experiments. The authors are also grateful to Tom Delworth (NOAA-Geophysical Fluid Dynamics Laboratory) for his insightful and helpful comments on a previous version of this paper.

References

An, S.-I., Wang, B., 2000. Interdecadal change of the structure of the ENSO mode and its impact on the ENSO frequency. J. Clim. 13, 2044–2055.
Balmaseda, M.A., Davey, M.K., Anderson, D.L.T., 1995. Decadal and seasonal dependence of ENSO prediction skill. J. Clim. 8, 2705–2715.
Chang, P., Ji, L., Li, H., 1997. A decadal climate variation in the tropical Atlantic Ocean from thermodynamics and air–sea interactions. Nature 385, 516–518.
Cooley, H., Ajami, N., Ha, M.-L., Srinivasan, V., Morrison, J., Donnelly, K., Christian-Smith, J., 2013. Global Water Governance in the 21st Century. Pacific Institute, Oakland, California.
Gleick, P.H., 1993. Water and conflict: fresh water resources and international security. Int. Secur. 18 (1), 112.
Hansen, J.E., et al., 2002. Climate forcing in Goddard Institute for Space Studies SI2000 simulations, J. Geophys. Res., 107, 4347, http://dx.doi.org/10.1029/2001JD001143.
Hidalgo, H.G., 2004. Climate precursors of multidecadal drought variability in the Western United States. Water Resour. Res. 40, W12504.
Houghton, R.W., Tourre, Y., 1992. Characteristics of low-frequency sea surface temperature fluctuations in the tropical Atlantic. J. Clim. 5, 765–771.
Keenlyside, N., Latif, M., Jungclaus, J., Kornblueh, L., Roeckner, E., 2008. Advancing decadal-scale climate prediction in the North Atlantic sector. Nature 453, 84–88.
Kestin, T.S., Karoly, D.J., Yano, J.-I., 1998. Time–frequency variability of ENSO and stochastic simulations. J. Clim. 11, 2258–2272.
Latif, M., Collins, M., Pohlmann, H., Keenlyside, N., 2006. A review of predictability studies of Atlantic sector climate on decadal time scales. J. Clim. 19, 5971–5987.
Mantua, N.J., Hare, S.R., Zhang, Y., Wallace, J.M., Francis, R.C., 1997. A Pacific decadal climate oscillation with impacts on salmon. Bull. Am. Meteorol. Soc. 78, 1069–1079.
McCabe, G.J., Palecki, M.A., Betancourt, J.L., 2004. Pacific and Atlantic Ocean influences on multidecadal drought frequency in the United States. Proc. Natl. Acad. Sci. 101, 4136–4141.
Meehl, G.A., Goddard, L., Murphy, J., Stouffer, R.J., Boer, G., Danabasoglu, G., Dixon, K., Giorgetta, M.A., Greene, A., Hawkins, E., Hegerl, G., Karoly, D., Keenlyside, N., Kimoto, M., Kirtman, B., Navarra, A., Pulwarty, R., Smith, D., Stammer, D., Stockdale, T., 2009. Decadal prediction: can it be skillful? Bull. Am. Meteorol. Soc. 90, 1467, http://dx.doi.org/10.1175/2009BAMS2778.1.
Meehl, G.A., Hu, A., 2006. Megadroughts in the Indian monsoon region and Southwest North America and a mechanism for associated multi-decadal Pacific sea surface temperature anomalies. J. Clim. 19, 1605–1623.
Mehta, V.M., Wang, H., Mendoza, K., 2014. Predictability of major decadal climate variability phenomena in CMIP5 experiments with the HadCM3, GFDL-CM2.1, NCAR-CCSM4, and MIROC5 global earth system models. J. Clim. (in preparation).
Mehta, V.M., Knutson, C.L., Rosenberg, N.J., Olsen, J.R., Wall, N.A., Bernadt, T.K., Hayes, M.J., 2013a. Decadal climate information needs of stakeholders for decision support in water and agriculture production sectors: a case study in the Missouri River basin. Weather Clim. Soc. 5, 27–42.
Mehta, V.M., Wang, H., Mendoza, K., 2013b. Decadal predictability of tropical basin-average and global-average sea-surface temperatures in CMIP5 experiments with the HadCM3, GFDL-CM2.1, NCAR-CCSM4, and MIROC5 global earth system models. Geophys. Res. Lett., 40, http://dx.doi.org/10.1002/grl.50236.
Mehta, V.M., Meehl, G., Goddard, L., Knight, J., Kumar, A., Latif, M., Lee, T., Rosati, A., Stammer, D., 2011. Decadal climate predictability and prediction: where are we? Bull. Am. Meteorol. Soc. 92, 637–640.
Mehta, V.M., 1998. Variability of the tropical ocean surface temperatures at decadal–multidecadal timescales, Part I: the Atlantic Ocean. J. Clim. 11, 2351–2375.
Mehta, V.M., Delworth, T., 1995. Decadal variability of the tropical Atlantic Ocean surface temperature in shipboard measurements and in a global ocean-atmosphere model. J. Clim. 8, 172–190.
Minobe, S., 1997. A 50–70 year climatic oscillation over the North Pacific and North America. Geophys. Res. Lett. 24, 683–686.
Murphy, J., Kattsov, V., Keenlyside, N., Kimoto, M., Meehl, G., Mehta, V., Pohlmann, H., Scaife, A., Smith, D., 2009. Towards prediction of decadal climate variability and change. In: Proceedings of an Invited White Paper for World Climate Conference, vol. 3, Geneva.
Nigam, S., Barlow, M., Berbery, E.H., 1999. Analysis links Pacific decadal variability to drought and streamflow in United States. EOS Trans. Am. Geophys. Union 80, 8.
Palmer, W.C., 1965. Meteorological Drought. Research Paper 45, Office of Climatology, Weather Bureau, Washington, DC, 58 pp.
Pohlmann, H., Jungclaus, J.H., Kohl, A., Stammer, D., Marotzke, J., 2009. Initializing decadal climate predictions with the GECCO oceanic synthesis: effects on the North Atlantic. J. Clim. 22, 3926–3938.
Power, S., Casey, T., Folland, C., Colman, A., Mehta, V.M., 1999. Interdecadal modulation of the impact of ENSO on Australia. Clim. Dyn. 15, 319–324.
Press, W.H., Teukolsky, S.A., Vetterling, W.T., Flannery, B.P., 1992. Numerical Recipes in Fortran 77, second ed. Cambridge University Press, Cambridge, UK.
Reynolds, R.W., Rayner, N.A., Smith, T.M., Stokes, D.C., Wang, W., 2002. An improved in situ and satellite SST analysis for climate. J. Clim. 15, 1609–1625.
Sato, M., Hansen, J., McCormick, M.P., Pollack, J., 1993. Stratospheric aerosol optical depth, 1850-1990. J. Geophys. Res 98, 22987–22994.
Schubert, S., et al., 2009. A US CLIVAR project to assess and compare the responses of global climate models to drought-related SST forcing patterns: overview and results. J. Clim. 22, 5251–5272.
Smith, D., Cusack, S., Colman, A., Folland, A., Harris, G., Murphy, J., 2007. Improved surface temperature prediction for the coming decade from a global circulation model. Science 317, 796–799.
Stenchikov, G., Hamilton, K., Stouffer, R.J., Robock, A., Ramaswamy, V., Santer, B., Graf, H.-F., 2006. Arctic Oscillation response to volcanic eruptions in the IPCC AR4 climate models. J. Geophys. Res., 111, D07107, http://dx.doi.org/10.1029/2005JD006286.
Tatebe, H., et al., 2012. Initialization of the climate model MIROC for decadal prediction with hydographic data assimilation. JMSJ Special issue on the recent development on climate models and future climate projections. JMSJ Special Issue on Recent Development on Climate Models and Future Climate Projections, 90A, 275–294.
Tyson, P.D., 1986. Climatic Change and Variability in Southern Africa. Oxford University Press, Oxford.
Wang, H., Mehta, V.M., 2008. Decadal variability of the Indo-Pacific warm pool and its association with atmospheric and oceanic variability in the NCEP-NCAR and SODA reanalyses. J. Clim. 21, 5545–5565.
Wells, N., Goddard, S., Hayes, M.J., 2004. A self calibrating palmer drought severity index. J. Clim. 17, 2335–2351.
Wilhite, D., 2000. Drought: A Global Assessment. Routledge, London.
Wilks, D.S., 1995. Statistical Methods in the Atmospheric Sciences. Academic Press, Oxford, UK 467 pp.